Detection of Antipersonnel Mines by Using the Factorization Method on Multistatic Ground-Penetrating Radar Measurements

Christian Fischer, Alexander Herschlein, Marwan Younis, *Member, IEEE,* and Werner Wiesbeck, *Fellow, IEEE*

***Abstract*—The factorization method (FM) has been applied to measurement data from a multistatic ground-penetrating radar operating in close proximity to the ground, which was used in a measurement campaign on the Joint Research Centre mine test lane in Ispra, Italy. This paper is targeted toward a future hand-held demining system. The according space limits restrict an independent positioning of transmit and receive antennas. Hence, very small multistatic datasets are obtained, representing a difficult case for the reconstruction with the FM.**

***Index Terms*—Angular diversity, antipersonnel mine, discrete complex image method (DCIM), factorization method (FM), Green's function, ground-penetrating radar (GPR), linear sampling method, multistatic radar, stratified media.**

I. Introduction

TODAY'S demining techniques like metal detectors, hand prodders, or mine dogs often are time consuming and fraught with risk. As a remedy, the idea of a hand-held multisensor system combining different physical sensor principles including a ground-penetrating radar (GPR) [1] has been the frame for this paper. However, the GPR application to antipersonnel mine (APM) detection is not straightforward, due to a number of physical or operational limitations [2], [3]. Many APMs are mostly dielectric objects with little metal content and a size less than 15 cm. This requires a very high spatial resolution. Lossy soils act as a frequency low-pass filter, whereas in low-loss soils, the dielectric contrast between the mine and the surroundings can be very low. In both cases, a very weak signal needs to be detected in the presence of strong disturbances and clutter. One approach to this problem involves human pattern recognition capabilities and learning experience. The system provides a reconstructed image of the ground, which is then interpreted by the operator.

The main idea in this paper is to apply a rather new nonlinearized image-formation scheme with low computational cost, which is the factorization method (FM) [4]. It is a modified version of the linear sampling method, which avoids erroneous reconstructions in special cases [5]. The FM relies on single-frequency "angular diversity" data [6], [7], which is a technological challenge, since it requires a multistatic radar system [8]–[11]. In this paper, an array of antennas mounted to a common carrier has been developed. Each antenna can act as transmitter and receiver, and all transmit/receive combinations in the array are measured.

This paper is organized as follows. The FM adaptation to a two-layer background and simulation tests is described in Section II. The realization of the multistatic GPR and system aspects such as calibration is covered in Section III. Measurement results in the laboratory and on the Joint Research Centre (JRC) mine test lane in Ispra are presented in Section IV.

II. FM

Imaging techniques for mine-detection GPR should be computationally efficient, should provide a good detection, localization, and discrimination of targets, and should account for the operational requirement (tripwires), that the radar's antennas need to be elevated above the ground, and therefore excite and measure the field in a medium (air) different from the one containing the targets.

Acoustic as well as electromagnetic problems in two and three dimensions has been treated with the FM so far [4], [12]. The solution space of the FM is restricted inherently: a qualitative image with scatterer boundaries and inhomogeneous areas present is generated, but quantitative values, e.g., dielectric permittivity, are not available. This restriction is at the same time an advantage of the FM: in contrast to other nonlinear methods, its computational effort is low, and hence, a real-time processing is an option even on a non-high-performance platform. An image is formed by evaluating an estimation function at test points (which can be irregularly spaced) in the area of interest. Large values of the estimation function indicate that the according test point is different from the background and, hence, belongs to a scatterer or an inhomogeneous area. The idea behind the method is to seek for a superposition of the scattered fields, such that the background Green's function is matched. The better the superposition succeeds for a test point, the higher the degree of affiliation to a scatterer.

Manuscript received October 3, 2005; revised April 23, 2006.

C. Fischer and A. Herschlein are with the EADS Astrium GmbH, 88039 Friedrichshafen, Germany.

M. Younis is with the German Aerospace Center (DLR), 82234 Oberpfaffenhofen, Germany.

W. Wiesbeck is with the Institut für Höchstfrequenztechnik und Elektronik, University of Karlsruhe (TH), 76128 Karlsruhe, Germany.

Digital Object Identifier 10.1109/TGRS.2006.883464

With the measurement data available in the so-called multistatic response matrix (MRM) $\mathbf{M}$, the estimation function Z for the point $\vec{x}_{\mathrm{B}}$ is calculated by [4]

$$Z(\vec{x}_{\mathrm{B}}) = \left[\sum_{i=1}^{N_i} \frac{\left|\mathbf{g}^*_{\vec{x}_{\mathrm{B}}} \psi_i\right|^2}{\sigma_i}\right]^{-1} \qquad \mathbf{g}_{\vec{x}_{\mathrm{B}}} = \begin{pmatrix} g(\vec{x}_{\mathrm{B}}, \vec{x}_{T,1}) \\ g(\vec{x}_{\mathrm{B}}, \vec{x}_{T,2}) \\ \vdots \\ g(\vec{x}_{\mathrm{B}}, \vec{x}_{T,i}) \end{pmatrix} \quad (1)$$

where N_i is the number of measurements, $\vec{x}_{T,i}$ is the according transmit antenna position, and $g(\vec{x}_{\mathrm{B}}, \vec{x}_{T,i})$ is the Green's function of the background medium. σ_i, and ψ_i are obtained from a singular-value decomposition of the MRM: $\mathbf{M} = \mathbf{\Phi}\Sigma\mathbf{\Psi}^{\mathrm{T}}$. ψ_i is the columns of the matrix $\mathbf{\Psi}^{\mathrm{T}}$, and σ_i is the singular values given by the diagonal matrix Σ.

Since all quantities in the above relations are frequency dependent, the reconstruction has to be performed for each excitation frequency separately.

A. MRM

In the (quadratic) MRM, the measurement data are collected. Each measurement value is sorted into the MRM in the order of the position of the Tx-antenna (defines the row) and the position of the Rx-antenna (defines the column). Thereby, monostatic measurements are located on the main diagonal. Since reciprocity can be assumed for a GPR in nearly all situations, the MRM is symmetric.

In the optimal case, the measurement system is able to completely fill up the MRM. It is reasonable to associate the MRM elements to a regular spatial grid over the target area. In practice, there is a dependence on the antenna arrangement and the sweeping trajectory of the platform, and not all combinations of Tx- and Rx-positions on the grid will be available. That is, certain parts of the MRM will remain unpopulated while others are covered multiple times. A practical system usually is a compromise of filling up the MRM as much as possible with the number of antennas available (see Section III-B).

Due to the nonlinear nature of the FM, the spacing of the measurement locations is not dictated by the Nyquist sampling theorem. Since no weighted summation of the antenna signals is performed, "grating lobes" do not exist. Instead, the reconstruction quality of the FM depends on the properties of the MRM, mainly its condition number and noise level.

B. Calculation of the Stratified Medium Green's Function

The scenario here is simplified by assuming a smooth and planar soil surface and homogeneous soil consisting of one or multiple planar stratified layers of lossy dielectric material. As shown from (1), each test point requires N_i times the evaluation of the Green's function (spatial domain) of the background medium. Its calculation therefore is crucial for the overall computational cost.

In this paper, the discrete complex image technique (DCIM) [13]–[15] is used, which has been implemented for the most relevant case of two-layered media. A straightforward extension to an arbitrary number of layers is possible by introducing generalized reflection and transmission factors [16]. In the two-layer case, four Green's functions, corresponding to source (excitation) and observation point being located either in the upper or lower medium, exist. The "transmission case," where source and observation point are located in different media, shall be discussed in the following.

The DCIM requires an approximation of the Fresnel transmission factors $T_{21}^{\perp,\parallel}$ (parallel $\parallel$ and perpendicular $\perp$ polarization) [16] of the form

$$T_{21}^{\perp,\parallel} e^{jk_{2z}z} \approx \sum_{n=1}^{N} a_{21n} e^{-b_{21n}k_{1z}} \quad (2)$$

where k_{1z} and k_{2z} are the perpendicular wavenumber components in the two layers and z is the antenna height above the interface. The approximation coefficients a_{21n} and b_{21n} in (2) are the unknowns to be determined. Using the Sommerfeld-Identity, an expression for the Green's function of the two-layered medium in the form of a weighted sum of free-space Green's functions is obtained

$$g_{21}^{\perp,\parallel}(\vec{x}, \vec{x}') = \sum_{n=1}^{N} a_{21n} \frac{e^{-jk_1 r_n(\vec{x}, \vec{x}')}}{4\pi r_n(\vec{x}, \vec{x}')} \quad (3a)$$

$$r_n(\vec{x}, \vec{x}') = \sqrt{(x - x')^2 + (z + z' - jb_{21n})^2} \quad (3b)$$

where $\vec{x}$ and $\vec{x}'$ are the position of the observation and the field excitation, respectively.

For the approximation (2), the Prony method or one of its variants has been proposed [13]. In this paper, better results were obtained using the generalized pencil-of-function method [14], [17]. The approximation for the Fresnel transmission factors $T_{21}^{\perp,\parallel}$ has been based on the approximation coefficients a_{11n} and b_{11n} for the Fresnel reflection factors $R_{21}^{\perp,\parallel}$ using the relations

$$T_{21}^{\perp} = R_{21}^{\perp} + 1 \quad T_{21}^{\parallel} = \sqrt{\frac{\varepsilon_1}{\varepsilon_2}} \left(R_{21}^{\parallel} + 1\right) \quad (4)$$

with dielectric permittivities ε_1 and ε_2. For perpendicular polarization, using (4), the transmission factor $T_{21}^{\perp}$ can be expressed by

$$T_{21}^{\perp} \approx \left(1 + \sum_{n=1}^{N_{11}} a_{11n} e^{-b_{11n}k_{1z}}\right) \quad (5)$$

where N_{11} is the approximation order used for the reflection factor. The remaining term in (2) to be approximated is

$$e^{jk_{2z}z} \approx \sum_{n=1}^{N'} a'_{21n} e^{-b'_{21n}k_{1z}}. \quad (6)$$

The determination of the coefficients a_{21n} and b_{21n} is possible by multiplying the two series (5) and (6). A comparison of series coefficients

$$\sum_{n=1}^{N} a_{21n} e^{-b_{21n}k_{1z}} = \left(1 + \sum_{n=1}^{N_{11}} a_{11n} e^{-b_{11n}k_{1z}}\right) \cdot \left(\sum_{n=1}^{N'} a'_{21n} e^{-b'_{21n}k_{1z}}\right) \quad (7)$$

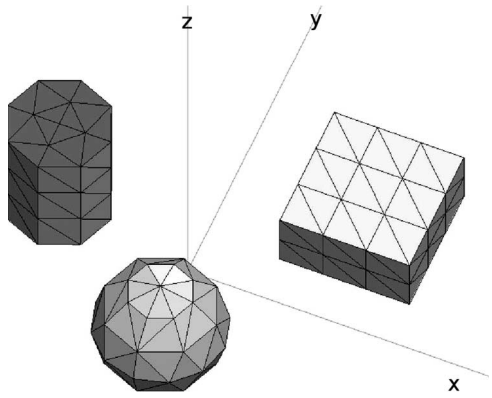

Fig. 1. Simulation scenario. Metallic cuboid (10-cm edges, height of 5 cm) centered at (−12 cm, 5 cm), metal sphere (radius of 5 cm) at (0 cm, −5 cm), and metal cylinder (radius of 4 cm, height of 10 cm) at (10 cm, 10 cm).

after multiplication of the two right-hand series results in the approximation coefficients a_{21n} and b_{21n}. In the same way, $T_{21}^{\|}$ can be approximated.

The calculation of the dyadic Green's function for planar stratified media [18] shall not be discussed in the frame of this paper. The measurement system (see Section III) only supports a single linear polarization, and a scalar implementation of the FM has been sufficient for all the reconstructions.

C. Numerical Test of the FM

Reconstructions of synthesized datasets have been performed to test the FM on severely limited datasets. Whereas in the literature [4], [12], typically, MRMs of size $\geq 30 \times 30$ were exploited for two-dimensional (2-D) reconstructions. It was anticipated in this paper that a multistatic GPR with these many antennas or spatial degrees of freedom would be of limited use for demining campaigns. Hence, it has been assumed that at maximum, an MRM of size 16×16 would be available, keeping in mind that three-dimensional (3-D) reconstructions were the goal.[1] A further limitation concerns the size of the usable aperture, which corresponds to the dimensions of the available antenna system (24 cm for the realized system, Section III-B). With such datasets, a scatterer shape reconstruction is expected to fail [19].

Full-wave forward simulations using the commercial moment-method code FEKO involved the repeated calculation of the scattered field in a scenario for different locations of transmit and receive antennas. In an experiment with 16 antenna locations, a total of 136 simulations (16 monostatic and 120 bistatic cases) had to be performed. To reduce the computation time, the scatterers were modeled as perfect electric conductor objects, transmit and receive antennas as $\lambda/2$-dipoles. Fig. 1 shows a setup of three objects embedded at 10-cm depth in a medium (not shown in the figure) with $\varepsilon_r = 10 - j0.1$, whereas the antennas are at a height of $z_{\mathrm{A}} = 0.15$ m. The simulation frequency was 1.7 GHz.

The reconstruction is shown in Fig. 2. As expected, the scatterer shapes are not reproduced, whereas localization and a certain discrimination are possible, since the image confirms that the scatterers have different shapes and sizes.

[1] It was considered impractical to use more than eight antennas in the realized hardware, hence, in the experiments, not even the 16×16 MRM could be fully populated (see Section III-B).

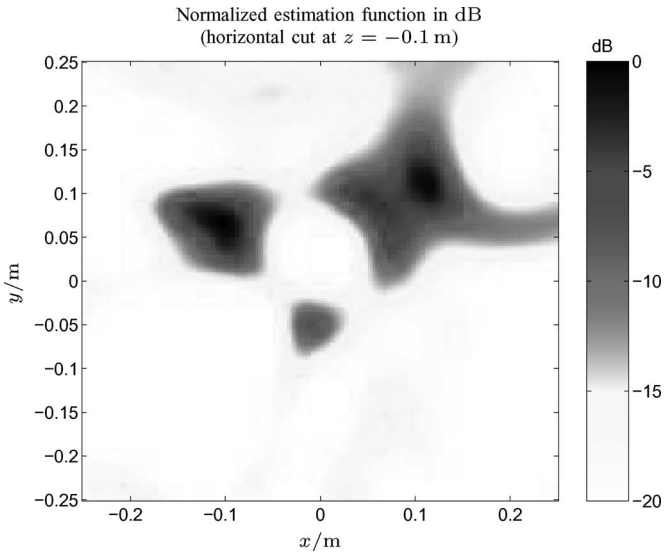

Fig. 2. Three-dimensional reconstructions of setup in Fig. 1 using FM. Targets embedded in material with $\varepsilon = 10 - j0.1$ at depth of 10 cm and antenna height of 15 cm.

III. Realized Hardware and System Aspects

In order to apply the FM to GPR in practice, a multistatic radar was developed. The system has been built around a vector network analyzer (VNA) operated as instrumentation radar.

A. Switching Matrix

Since the available VNA was equipped with a two-port test set, only two monostatic (reflection) and one bistatic (transmission) measurement would have been possible by connecting an antenna to each test-set port. Hence, a switching matrix as a link between the VNA and up to eight antennas was built. It can be operated up to 3 GHz, and it shows a decoupling between all ports of better −40 dB and a two-way signal attenuation < 8 dB.

B. Antenna Configuration and Multistatic Array Operation

The main antenna design driver has been weighted and sized, since multiple antennas needed to be attached to a platform of limited size with a weight suited for a hand-held operation. A wide frequency band of operation starting from low frequencies should be possible to be flexible during the tests. For these reasons, exponentially tapered slot (Vivaldi) antennas have been designed and built. The result is a radiator with 7 : 1 bandwidth (0.7–4.8 GHz) at a return loss < -10 dB. The average gain in the operating frequency range is 4.5 dB, and the cross polarization is < -19 dB.

As it has been mentioned, in a practical hand-held system, the number of antennas is limited, and hence, it needed to be examined whether sufficient input data could be provided for the FM. The idea was to combine a platform motion with the available radar channels to synthesize additional channels. For each position of the antenna carrier, only 36 channels

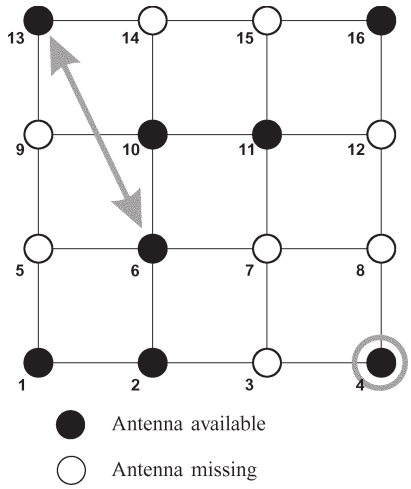

Fig. 3. Optimal configuration of eight antennas on a 4 × 4 grid. Monostatic operation of antenna no. 4 and bistatic operation of antennas 6 and 13 are highlighted as examples to be found in Fig. 4.

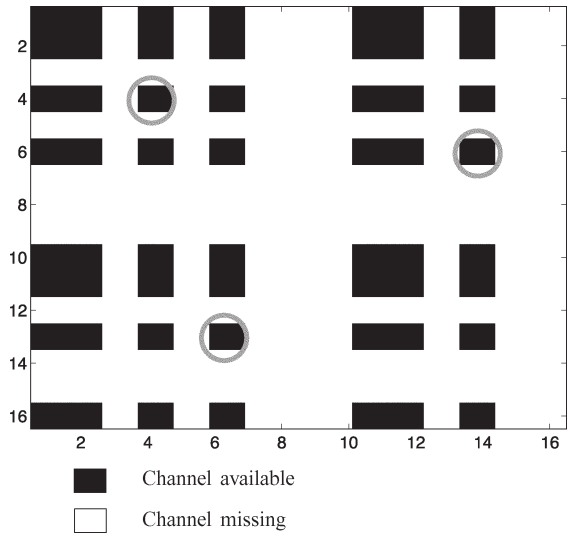

Fig. 4. Population of 16 × 16 MRM for fixed antenna system. Matrix positions related to monostatic operation of antenna no. 4 (circle on main diagonal) and bistatic operation of antennas 6 and 13 are highlighted as examples.

(eight mono- and 28 bistatic ones) resulting in an 8 × 8 MRM are available. Once the antenna carrier is swept across the ground, further channels can be covered. Each position where a measurement by any of the antennas takes place adds one row and one column to the MRM. If an unwise strategy is chosen, a large but only sparsely populated MRM results, which is badly suited for the FM. In contrast, the aim is an as-large-as-possible but densely populated MRM, which is possible in the special case when the measurements of the swept antenna system are carried out on a regular grid with a spacing equal to the separation between the antennas. This implies that the antennas are mounted according to a regular grid on the antenna carrier. In practice, an operator will not be able to move the antenna system along a regular grid with the necessary precision. For the time being, this topic has not been the focus of this paper.

The favorable antenna arrangement to populate a 16 × 16 MRM as fully as possible with eight antennas available is shown in Fig. 3. For a fixed carrier location, the 16 × 16 MRM

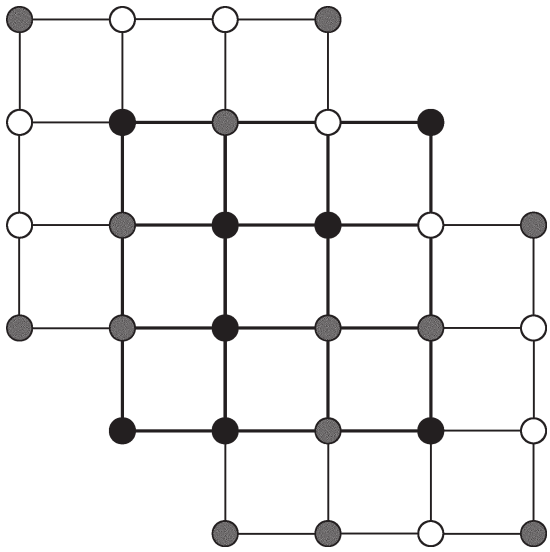

Fig. 5. Overlaying of channels for moving antenna system. Black circles indicate antennas on the carrier in starting position. Gray circles are antenna positions which have been reached by moving the carrier, and white circles relate to positions which are uncovered.

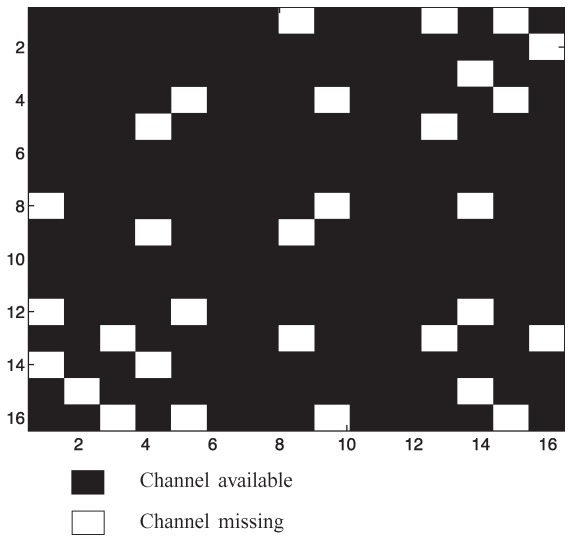

Fig. 6. Population of 16 × 16 MRM for moving antenna system.

can be filled to the degree shown in Fig. 4. In conjunction with the platform motion, the channels can be overlaid as indicated in Fig. 5, resulting in the MRM of Fig. 6 with 242 of 256 matrix positions populated. This is achieved by scanning the platform over a 6 × 5 grid.

The antenna system realized according to the described strategy is shown in Fig. 7. The underlying grid has a spacing of 8 cm; hence, the outer antennas are 24-cm apart. The antennas are tilted so they all cover the same footprint on the ground.

C. System Calibration

Systematic error influences, e.g., antenna coupling, interactions between antennas and soil and ground surface scattering, are severe for a GPR and pose two calibrations tasks.

1) Calibration of the frequency response of the system [20], [21], e.g., due to transmit–receive path coupling,

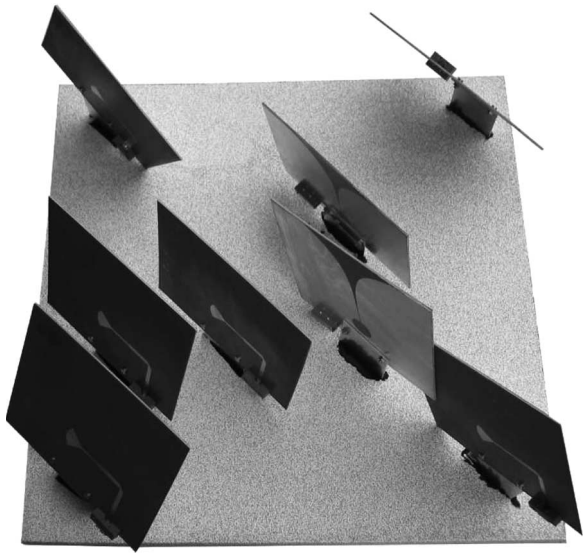

Fig. 7. Realized multistatic antenna system.

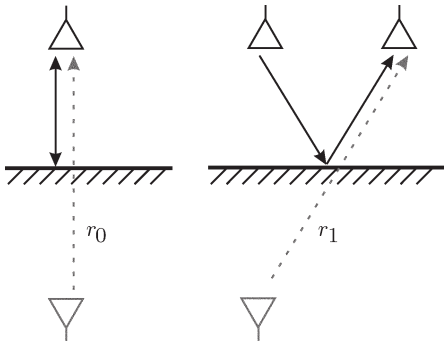

Fig. 8. Metallic plate as reference for system angular response.

nonideal components, etc. Since the FM operates on single-frequency data, in this paper, the system's frequency response could be neglected.

2) Calibration of the system's angular response, i.e., relative amplitude and phase relations among the channels, which is crucial for the multistatic system.

A large metallic plate, placed directly onto the soil surface and then varied in height, is proposed in [21] as a reference target (reflection factor $S^{\mathrm{p}} = -1$) to calibrate the frequency response of the system. If this calibration was performed on all channels of a multistatic system, the response of the reference target at the reference position would be identical in all channels, and hence, the amplitude/phase relations due to the different antenna locations would be lost.

Here, the large metallic reference plate has been used for interchannel phase calibration by multiplying the reflection factor with a phase factor expected from the geometric position of the antennas (image theory), as shown in Fig. 8. The resulting target reflection factor is $S^{\mathrm{p}} = -1 \cdot e^{jk(r_0 - r_1)}$.

IV. Measurement Results

A. Laboratory Verification

The eight-antenna system has first been tested in a laboratory setup to validate the proper function of all 36 channels. A two-axis positioning system with 0.25-mm accuracy covering an area of 1.6 × 0.6 m has been used to move the antenna carrier. A functional test of the 36 different channels of the antenna system has been performed by reconstructing images for each channel separately using a microwave tomography.

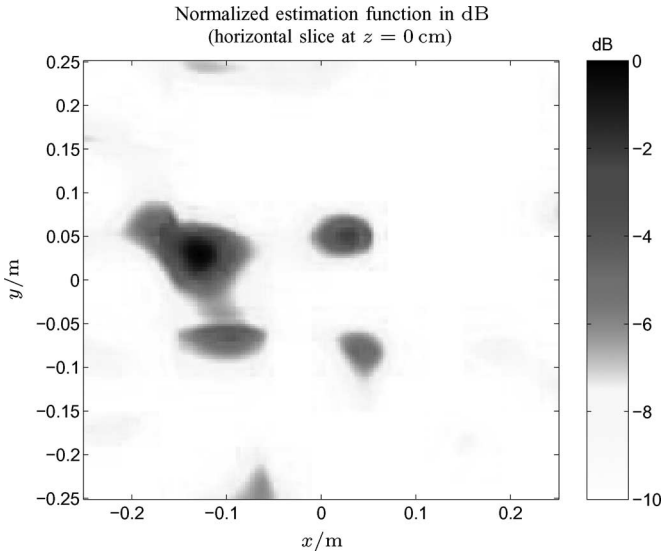

Fig. 9. Extension of the reconstructed area of the FM by stacking the subimages. CW frequency of 3.04 GHz and antenna height of 29 cm.

Fig. 9 shows the FM reconstruction of a free-space scenario of four metallic targets (upper left: disk with 5-cm diameter, others: spheres with 3.6-cm diameter). Since the lateral extent of the reconstructed area is larger than the area covered by the measurements in the optimal MRM of size 16 × 16, overlapping subapertures have been used, which result in smaller images shifted by the measurement grid size. By stacking these subimages, the total image was obtained. This procedure can be extended to arbitrarily large images; it also introduces averaging, which improves the image quality.

B. Test Mine Field of the European Commission JRC

The European Commission JRC in Ispra, Italy, has been hosting the "Joint Multi-Sensor Mine Signature Measurement Campaign," which took place from 1999 to 2003 [22]. For this project, a test area has been set up to allow trials with different sensors designed for the detection of antipersonnel mines. The test field consists of a long lane, which has been divided in several "plots." The plots differ in soil type but contain exactly the same layout of targets and false targets.

The described multistatic system was used for a measurement campaign in April 2003. The performance in different soil types was investigated: loamy soil with low clutter content (plot 2), sandy soil (plot 3), pure sand (plot 4), clay (plot 5), and ferromagnetic soil (plot 7). The antenna system together with the two-axis positioner has been attached to a large movable bridge which was used for coarse positioning of the system on the test site. The setup is shown in Fig. 10. The antennas were at a height of 10 cm above the ground. Due to the slow acquisition speed of the VNA—measurements had to be performed in a time-consuming step-by-step manner—and the limited scan area of the positioning system, a limitation to

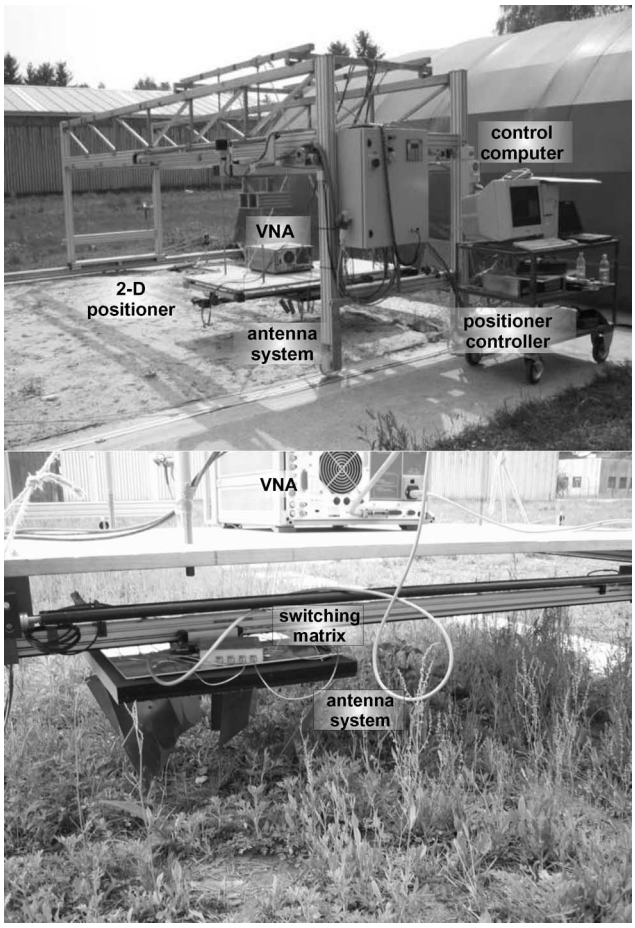

Fig. 10. Measurement setup.

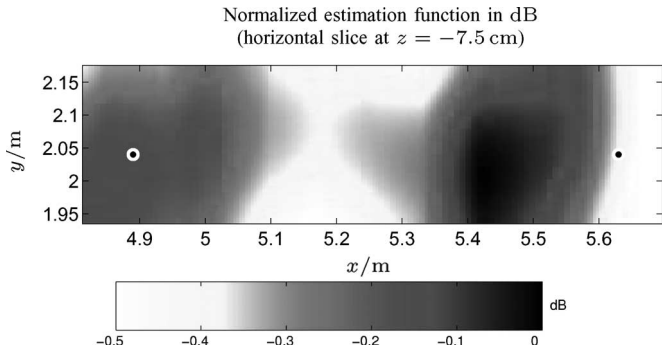

Fig. 11. Plot 2C using FM (regularization parameter $\alpha = 10^{-2}$), M3A and M3B at $x = 4.89$ m and $x = 5.63$ m, $y = 204$ cm, depth of -5 cm. CW frequency of 728 MHz and Green's function with 32 images.

rectangular patches of 0.3-m^2 size inside the 36-m^2 plots had to be made. Since the target layout in the plots is rather sparse, the covered areas of 96 $\times$ 32 cm were just large enough to cover two targets separated by a distance of 74 cm. The x direction belongs to the (longer) east–west dimension in the images (Figs. 11–13), while y is related to the shorter north–south dimension. The processing time under MATLAB on an AMD Athlon XP 1600+ system with 512 MB of RAM running RedHat Linux was approximately 150 s, including the DCIM approximation of the Green's function with 32 images. A regularization scheme as described in [23] has been used for the FM. Although the humidity and temperature of the soil of

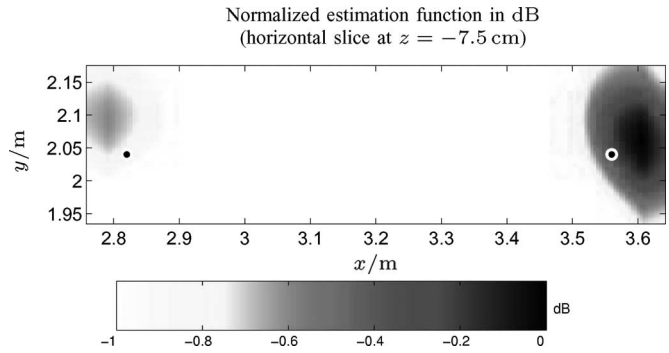

Fig. 12. Plot 5B using FM (regularization parameter $\alpha = 10^{-2}$), M3A and M3B at $x = 2.82$ m and $x = 3.56$ m, $y = 204$ cm, depth of -5 cm. CW frequency of 784 MHz and Green's function with 32 images.

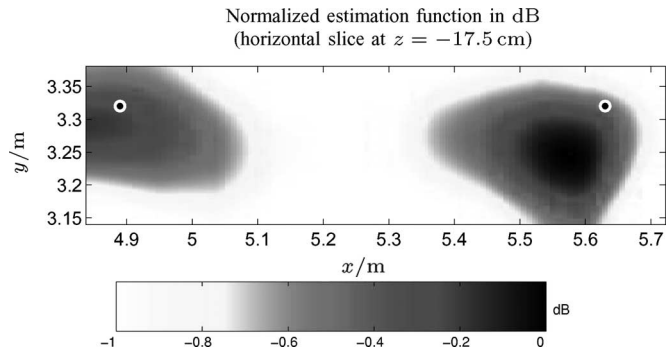

Fig. 13. Plot 5C using FM (regularization parameter $\alpha = 10^{-2}$), M3A and M3B, at $x = 4.89$ m and $x = 5.63$ m, $y = 332$ cm, depth of -15 cm. CW frequency of 700 MHz and Green's function with 32 images.

the plots have been logged during the measurements, no exact model for the soil properties of the test lane plots is available. With an average humidity of around 10% during the campaign, the soil properties have been estimated using a standard model to $\varepsilon = 6.3 - j0.1$ [24]. The fact that the exact soil properties have not been available introduces a systematic which may be partly responsible for localization errors in the following examples.

Fig. 11 is a reconstruction of a measurement in the loamy soil of plot 2. Two targets buried at a depth of 5 cm (target top to soil distance) are expected to appear at $x = 4.89$ m and $x = 5.63$ m, both at $y = 2.04$ m. Both targets have a diameter of 10 cm. The left target has less metal content than the right one. As it is seen, the dynamic range of the estimation function is very small, and the target reconstruction is blurred. The left target however is visible around its expected position, whereas the right target appears superposed by a strong clutter level in the area around $x = 5.45$ m.

A reconstruction in the clay soil of plot 5 ($\varepsilon = 6.3 - j0.1$ assumed) is shown in Fig. 12. The targets, only 5 cm in diameter, are expected at $x = 2.82$ m and $x = 3.56$ m, both at $y = 2.04$ m. Again, the dynamic range of the estimation function is rather low, but both mine dummies appear as strongest targets, clearly visible above the clutter level. The left target, which has less metal content, is reconstructed as weaker target.

As a final example, the reconstruction of two targets buried at a greater depth of 15-cm clay soil is shown in Fig. 13. Even

under these difficult conditions, the targets still are visible and localized above the clutter level.

V. Conclusion

In this paper, the factorization method in a 3-D version with a two-layer background has been applied to measurement data from a GPR in close proximity to the ground. The Green's function of the background has been calculated efficiently using the discrete complex image method. A multistatic GPR has been realized, which was used in a measurement campaign on the JRC mine test lane in Ispra, Italy. The respective GPR was designed with a hand-held operation in mind, which means that severe limitations concerning the positioning of transmit and receive antennas are faced. In the present case, an irregular arrangement of eight antennas on a common carrier has led to single-frequency datasets of very limited volume, i.e., 136 complex values. Under these circumstances, the FM performance is low but appears sufficient to allow for scatterer detection.

Of particular interest for future work is the question: how using a hand-held GPR approach can more degrees of freedom in the antenna positioning be achieved to obtain larger datasets with more angular-diversity information. Irregular scan trajectories will require further examination, e.g., interpolation techniques, to transform the resulting large but sparsely populated multistatic response matrices to smaller size and dense population. The use of frequency diversity will likely prove valuable by combining reconstructions at different excitation frequencies to increase the knowledge about a scenario.

Acknowledgment

The authors would like to thank A. Kirsch, the inventor of the factorization method, who has been the most valuable discussion partner and adviser concerning the presented work. The authors would also like to thank A. Lewis (European Commission Joint Research Centre, Ispra, Italy) for hosting the measurement campaign on the "Multi-Sensor Mine Signature" test field.

References

[1] D. J. Daniels, *Surface Penetrating Radar*. London, U.K.: IEE Press, 1996.

[2] P. Blagden, "Mine detection and the need for new technology," *Forum Phys. Soc. Amer. Phys. Soc.*, vol. 31, no. 3, pp. 8–11, Jul. 2002.

[3] *Mine Action Equipment: Study of Global Operational Needs*, 2002, Geneva, Switzerland: Geneva Int. Centre Humanitarian Demining. Report.

[4] A. Kirsch, "The MUSIC-algorithm and the factorization method in inverse scattering theory for inhomogeneous media," *Inv. Probl.*, vol. 18, no. 4, pp. 1025–1040, Aug. 2002.

[5] A. Liseno and R. Pierri, "Impossibility of recovering a scatterer's shape by the first version of the 'linear sampling method'," *Int. J. Electron. Commun. (AEU)*, vol. 57, no. 1, pp. 70–73, Jan. 2003.

[6] R. Pierri, R. Persico, and R. Bernini, "Information content of the Born field scattered by an embedded slab: Multifrequency, multiview, and multifrequency-multiview cases," *J. Opt. Soc. Amer. A, Opt. Image Sci.*, vol. 16, no. 10, pp. 2392–2398, Oct. 1999.

[7] O. M. Bucci, L. Crocco, T. Isernia, and V. Pascazio, "Subsurface inverse scattering problems: Quantifying qualifying and achieving the available information," *IEEE Trans. Geosci. Remote Sens.*, vol. 39, no. 11, pp. 2527–2537, Nov. 2001.

[8] D. E. Lynch, R. D. Brown, D. D. Mokry, J. van Damme, R. A. Schneible, and M. C. Wicks, "Multistatic ground penetrating high frequency radar," in *Proc. 5th Int. Conf. Radar Syst.*, Brest, France, May 1999, pp. 1056–1059.

[9] B. Sai and L. P. Ligthart, "High resolution 3D imaging reconstruction based on multistatic UWB phase processing," *Proc. SPIE*, vol. 4491, pp. 68–78, Jul. 2001.

[10] D. J. Daniels, D. Brooks, J. Dittmer, O. Mitchell, and N. Hunt, "Wide swath multi-channel GPR systems for mine detection," in *Proc. Radar*, Edinburgh, U.K., Oct. 2002, pp. 210–216.

[11] G. Alberti, L. Ciofaniello, G. Galiero, R. Persico, M. Sacchettino, and S. Vetrella, "A stepped frequency GPR system working both ungated and gated mode," in *Proc. Workshop 'Radar a Bassa Frequenza'*, Napoli, Italy, 2001, pp. 1–11.

[12] D. Colton, J. Coyle, and P. Monk, "Recent developments in inverse acoustic scattering theory," *SIAM Rev.*, vol. 42, no. 3, pp. 369–414, 2000.

[13] Y. L. Chow, J. J. Yang, D. G. Fang, and G. E. Howard, "A closed-form spatial Green's function for the thick microwave substrate," *IEEE Trans. Microw. Theory Tech.*, vol. 39, no. 3, pp. 588–592, Mar. 1991.

[14] M. I. Aksun, "A robust approach for the derivation of closed-form Green's functions," *IEEE Trans. Microw. Theory Tech.*, vol. 44, no. 5, pp. 651–658, May 1996.

[15] Y. Liu, L.-W. Li, T.-S. Yeo, and M.-S. Leong, "Application of DCIM to MPIE-MoM analysis of 3-D PEC objects in multilayered media," *IEEE Trans. Antennas Propag.*, vol. 50, no. 2, pp. 157–162, Feb. 2002.

[16] W. C. Chew, *Waves and Fields in Inhomogeneous Media*. Piscataway, NJ: IEEE Press, 1995.

[17] Y. Hua and T. K. Sarkar, "Matrix pencil method for estimating parameters of exponentially damped/undamped sinusoids in noise," *IEEE Trans. Acoust., Speech, Signal Process.*, vol. 38, no. 5, pp. 814–824, May 1990.

[18] W. Cai and T. Yu, "Fast calculations of dyadic Green's functions for electromagnetic scattering in a multilayered medium," *J. Comput. Phys.*, vol. 165, no. 1, pp. 1–21, Nov. 2000.

[19] A. Liseno and R. Pierri, "Shape reconstruction by the spectral data of the far-field operator: Analysis and performances," *IEEE Trans. Antennas Propag.*, vol. 52, no. 3, pp. 899–903, Mar. 2004.

[20] W. Wiesbeck and S. Riegger, "A complete error model for free space polarimetric measurements," *IEEE Trans. Antennas Propag.*, vol. 39, no. 8, pp. 1105–1111, Aug. 1991.

[21] V. A. Mikhnev and P. Vainikainen, "Single-reference near-field calibration procedure for step-frequency ground penetrating radar," *IEEE Trans. Geosci. Remote Sens.*, vol. 41, no. 1, pp. 75–80, Jan. 2003.

[22] P. Verlinde and A. Lewis, "MSMS introduction," *Joint Multi-Sensor Mine Signature Measurement Campaign*, 2003, Ispra, Italy: Eur. Commission Joint Res. Centre. accessed Nov. 6, 2006. [Online]. Available: http://demining.jrc.it/msms/

[23] A. Kirsch, "Characterization of the shape of a scattering obstacle using the spectral data of the far field operator," *Inverse Probl.*, vol. 14, no. 6, pp. 1489–1512, Dec. 1998.

[24] F. T. Ulaby, R. K. Moore, and A. K. Fung, *Microwave Remote Sensing: Active and Passive*, vol. II. Reading, MA: Addison-Wesley, 1982. Advanced Book Program.

Christian Fischer was born in Karlsruhe, Germany, in 1970. He received the Dipl.-Ing. (M.S.E.E.) and the Dr.-Ing. (Ph.D.E.E.) degrees in electrical engineering from the University of Karlsruhe (TH), Karlsruhe, in 1997 and 2003, respectively.

From 1997 to 2003, he was a Research Scientist with the Institut für Höchstfrequenztechnik und Elektronik, University of Karlsruhe (TH). During this period, his research activities included ground-penetrating radar, RCS measurements, antenna development, wave propagation, and field theory. Since 2004, he has been with the Optical and Microwaves Department of EADS Astrium, Friedrichshafen, Germany, where he has been working in the field of spaceborne SAR system engineering, SAR performance prediction, and technology for future spaceborne SAR systems.

Alexander Herschlein received the Dipl.-Ing. (M.S.E.E.) and the Dr.-Ing. (Ph.D.E.E.) degrees from the University of Karlsruhe, Karlsruhe, Germany, in 1993 and 2002, respectively.

From 1994 to 2002, he was with the Institut für Höchstfrequenztechnik und Elektronik, University of Karlsruhe (TH), where he was a Research Assistant responsible for lectures in antennas and antenna systems. His research responsibilities during this period included field theory, numerical methods, optimizations, wave propagation, antennas, and EMC. From 1998 to 1999, he also worked for DaimlerChrysler AG, Research Center Ulm, Germany. Since 2003, he has been with EADS Astrium in Friedrichshafen, Germany, where he has been engaged in microwave system engineering. He is the Head of the antenna laboratory, responsible for antenna designs and optimizations, RF test definitions, and RF measurements. His main topic is the optimization of the active TerraSAR-X antenna, and he is the Leader of the measurement campaign of this phased array.

Marwan Younis (S'95–M'04) was born in Las Cruces, NM, in 1970. He received the Dipl.-Ing. (M.S.E.E.) and the Dr.-Ing. (Ph.D.E.E.) degrees in electrical engineering from the University of Karlsruhe (TH), Karlsruhe, Germany, in 1997 and 2004, respectively.

From 1998 to 2004, he was a Research Scientist with the Institut für Höchstfrequenztechnik und Elektronik, University of Karlsruhe (TH). Since 2001, he has been a Lecturer for advanced radio communication with the Universität Karlsruhe (TH). In 2005, he joined the Microwave and Radar Institute of the German Aerospace Center (DLR), Oberpfaffenhofen, Germany. He has authored a number of conference papers and peer-reviewed publications. His research fields include SAR systems, digital beam forming for radar, synchronization of bistatic SAR, forward looking radar, and antennas.

Dr. Younis has served as a Treasurer and Chair of the IEEE Student Branch in Karlsruhe. He received the Hermann-Billing Award for his Ph.D. thesis in 2005.

Werner Wiesbeck (SM'87–F'94) received the Dipl.-Ing. (M.S.E.E.) and the Dr.-Ing. (Ph.D.E.E.) degrees from the Technical University Munich, Munich, Germany, in 1969 and 1972, respectively.

From 1972 to 1983, he was with AEG-Telefunken in various positions including the Head of R&D of the Microwave Division in Flensburg and Marketing Director of the Receiver and Direction Finder Division, Ulm. During this period, he had product responsibility for millimeter-wave radars, receivers, direction finders, and electronic warfare systems. Since 1983, he has been the Director with the Institut für Höchstfrequenztechnik und Elektronik (IHE) at the University of Karlsruhe (TH), Karlsruhe, Germany, where he had been a Dean of the Faculty of Electrical Engineering. His research topics include radar, remote sensing, wireless communication, and antennas. In 1989 and 1994, respectively, he spent a six-month sabbatical at the Jet Propulsion Laboratory, Pasadena, CA.

Prof. Wiesbeck is a member of the IEEE GRS-S AdCom (1992–2000), Chairman of the GRS-S Awards Committee (1994–1998, 2002–present), Executive Vice President IEEE GRS-S (1998–1999), President IEEE GRS-S (2000–2001), Associate Editor IEEE TRANSACTIONS ON ANTENNAS AND PROPAGATION (1996–1999), past and present Treasurer of the IEEE German Section (1987–1996, 2003–2007). He has been a General Chairman of the '88 Heinrich Hertz Centennial Symposium, the '93 Conference on Microwaves and Optics (MIOP '93), the Technical Chairman of the International mm-Wave and Infrared Conference 2004, Chairman of the German Microwave Conference GeMIC 2006, and he has been a member of the scientific committees and TPCs of many conferences. For the Carl Cranz Series for Scientific Education, he serves as a permanent Lecturer for radar system engineering, wave propagation, and mobile communication network planning. He is a member of an Advisory Committee of the EU—Joint Research Centre (Ispra/Italy), and he is an Advisor to the German Research Council (DFG), to the Federal German Ministry for Research (BMBF), and to industry in Germany. He is the recipient of a number of awards, lately the IEEE Millennium Award, the IEEE GRS Distinguished Achievement Award, the Honorary Doctorate (Dr. h.c.) from the University Budapest/Hungary, and the Honorary Doctorate (Dr.-Ing. E.h.) from the University Duisburg/Germany. He is an Honorary Life Member of the IEEE GRS-S, a member of the Heidelberger Academy of Sciences, and a member of Acatech (German Academy of Engineering and Technology).